Effects of Rib-Configuration in the Thermal Performance of One-sided Heated, Rib-Roughened Cooling Channels

Sebastian Ruck, Frederik Arbeiter

Institute of Neutron Physics and Reactor Technology, Karlsruhe Institute of Technology

Address and correspondence to Dr. Sebastian Ruck, Karlsruhe Institute of Technology, Institute of Neutron Physics and Reactor Technology, Hermann-von-Helmholtz-Platz 1, Building 521, 76344 Eggenstein-Leopoldshafen, Germany
sebastian.ruck@kit.edu
Phone number: +49 721 608-29279, Fax number: +49 721 608-23718

ABSTRACT

Detached-Eddy-Simulations (DES) were performed for investigating the thermal-hydraulics of a one-sided heated and rib-roughened cooling channel at Reynolds numbers ranging from $2.5 \cdot 10^4$ to $1.58 \cdot 10^5$. Heat transfer and flow characteristics for three different types of centrally positioned, transversally oriented rib-elements with a rib-height and rib-top-width of e and (a) 90 deg. edged, (b) 2 e radius round-edged or (c) 30 deg. inclined front- and rear-rib-surface haven been analyzed. The rib-pitch-to-rib-height-ratio was p/e = 10 and the rib-height-to-hydraulic-diameter-ratio was e/D_h = 0.0638. For all simulations, friction factors decrease and heat transfer coefficients increase for increasing Reynolds numbers. For varying rib-shapes, the averaged friction factor ratios differ up to 30 pct. and the Nusslet Numbers at the rib-roughened and the overall Nusselt Numbers differ up to 12 pct. and 8 pct., respectively. Maximum flow resistance and heat transfer occur for the 90 deg. edged rib-configuration. For all rib-shapes, the thermal performance factor (of increased heat conductance and equal pumping power) for cooling the rib-roughened wall decreases for increasing Reynolds numbers. Best thermal performance was obtained for the 90 deg. edged rib-configuration. Correlations for Nusselt number and average friction factor prediction were derived for the entire Reynolds number range.

INTRODUCTION

Rib-roughened channel walls enhance the heat transfer of internal cooling passages and are frequently applied in heat exchanger and cooling applications, i.e. gas turbine blade cooling or gas-cooled reactors. Corresponding flow and heat transfer phenomena have been studied for decades. Focusing on heat transfer enhancement mechanism, flow motion, mean velocity distributions, turbulent fluctuations and friction factor development, flows in heated channels with one- and two-sided, opposite rib-roughened walls of transversally oriented rib-elements were determined by LDA [1-4] and pressure drop measurement techniques or computed by Large- and Detached-Eddy-Simulation techniques [5-9]. Corresponding temperature field measurements were carried out by thermocouple probes, liquid-crystal thermometry [1] and holographic interferometry [2-4]. For global performance estimations the effects of varying flow conditions and rib-designs on heat transfer and flow characteristics were studied systematically by means of pressure drop and wall temperatures measurements [10-16].

The present work aims at improved designs of high-pressure helium-gas running internal cooling passages for high heat flux components of fusion, nuclear or solar power plants. Detached-Eddy-Simulations (DES) were performed for investigating the thermal-hydraulics of a one-sided and heated rib-roughened cooling channel with three different types of centrally positioned, transversally oriented rib-elements at Reynolds numbers, $Re = (\dot{m} \cdot D_h)/(A \cdot \mu)$, ranging from $2.5 \cdot 10^4$ to $1.58 \cdot 10^5$. The thermal-hydraulic conditions and the computational domain correspond to the so-called HETREX experiment (at KIT, Germany) for pressure drop and heat transfer prediction. The presented computations provide additional results of spatially averaged heat and flow characteristics, which are not resolved by the experiments.

METHODS

Detached Eddy Simulation

In the last years, DES has been established as a reliable computational method for turbulent flows of massive separation. It was successfully applied for thermal-hydraulic predictions in two-sided rib-roughened channels at $Re = 2\cdot10^4$ [8,9] (with reduced numerical cost of about one order of magnitude compared to LES). DES is a non-zonal hybrid RANS/LES approach assigning RANS to attached boundary layer flows and LES to separated flow regions. Initially, it was introduced with the S-A turbulence model [17], the so-called DES97, and extended to the k-ω-SST model [18,19]. In general, the DES methodology bases on implementing a DES limiter to a RANS turbulence model. The limiter is controlled by the local grid size (Δx, Δy, Δz) and turbulence flow length l_t inducing the switching between the LES and RANS mode. For introducing the k-ω-SST model into the DES approach the dissipative term of the k-equation was modified. The turbulent flow length scale $l_t^k = k^{1/2}/(\beta^* \cdot \omega)$ of the dissipative term is substituted by a new DES length scale $l_t^{DES} = \min[l_t^k, C_{DES}^k \cdot \Delta]$ with the DES constants C_{DES}^k and the filter width $\Delta = \max(\Delta x, \Delta y, \Delta z)$. The DES constant C_{DES}^k shifts between the k-ω and k-ε branch of the k-ω-SST model. In regions where the maximum spatial grid spacing is much larger than the flow turbulence length scale, DES functions in RANS mode with the conventional k-ω-SST formulation [20] and in regions of comparable small maximum spatial grid spacing, DES functions in LES mode and the eddy-viscosity is calculated by a subgrid-scale like model formulation of $\nu_{SGS} = k_{SGS}/\omega$. In the present study the delayed DES approach with k-ω-SST model [21], the DES constant of $C_{DES}^{k-\varepsilon} = 0.61$ and of $C_{DES}^{k-\omega} = 0.78$ and the turbulent Prandtl number of $Pr_t = Pr_{SGS} = 0.85$ were used.

Computation, Boundary Conditions and Simulation Details

The computational domain was derived from the HETREX (Heat TRansfer Enhancement eXperiements) test section. It represents a section of the experimental setup (for corresponding pointwise heat transfer and pressure drop measurements) and contains a fluid and a solid domain as displayed in Fig 1. The solid domain consists of the structure walls and the heating unit below the rib-roughened channel with a cylindrical heater cartridge. The fluid domain of the cooling channel contains the one-side heated and rib-roughened channel zone and a non-heated smooth outlet zone with identical channel dimensions. The rib-roughened channel zone is structured by 16 centrally positioned, transversally oriented rib-elements with a rib-height and rib-top-width of e and (a) 90 deg. edged (TE), (b) 2 e radius round-edged (TR) or (c) 30 deg. inclined (TI) front- and rear-rib-surface, see Fig. 2. The channel cross section is 15 e x 15 e with 2 e inside radiuses, the rib-pitch-to-rib-height-ratio is p/e=10, the rib-height-to-hydraulic-diameter-ratio is e/D_h = 0.0638 and the rib-width-to-channel-width-ratio is L_e/W = 0.6 (TE) and 0.82 (TR, TI), as illustrated in Fig 2. The present channel was designed for channel- and rib-manufacturing by ordinary mill cutting with spherical and cylinder head cutters.

The simulations were carried out for Reynolds numbers Re and heat up rates $q^+ = q \cdot A/\dot{m} \cdot c_p(T) \cdot T_{in}$ of (Re; q^+) = ($2.5 \cdot 10^4$; $4.5 \cdot 10^{-3}$), ($5.1 \cdot 10^4$; $2.1 \cdot 10^{-3}$), ($7.75 \cdot 10^4$; $1.45 \cdot 10^{-3}$), ($1.1 \cdot 10^5$; $1.0 \cdot 10^{-3}$) and ($1.58 \cdot 10^5$; $7.1 \cdot 10^{-4}$). The thermal-hydraulic conditions represent common operating ranges of high pressure helium-gas running cooling channels of planned fusion reactors or helium-/air-gas- or thermo-oil-running absorber tubes of solar receivers. The fully turbulent developed inflow conditions were obtained separately by periodic, isothermal DES of a smooth channel fluid domain with identical dimensions as the channel inlet. Adiabatic boundary conditions were assumed for the outer walls of the solid domain and a constant heat flux density was applied at the heater cartridge surface of the solid domain. The fluid was air (at p_{in} = 0.4 MPa(abs) and T_{in} = 293.15 K) with ideal gas conditions and temperature dependent density $\rho(T)$, specific heat capacity $c_P(T)$, thermal conductivity $\kappa(T)$ and fluid viscosity $\nu(T)$ [22]. The compressible fluid conditions yield slight axial change of the Reynolds numbers. The solid was stainless steel [X6CrNiMoTi17-12-2 (316Ti)] with a constant density of ρ^{316Ti} = 7980 kg/m^3 and temperature dependent material parameters $c_p^{316Ti}(T)$ and $\kappa^{316Ti}(T)$ [22].

Local grid refinement was performed in the vicinity of the rib-elements and within the inter-rib-spacing resulting in a focus region aiming on maximum cells sizes of $\Delta x^+ \approx 11$ and $\Delta y^+ \approx \Delta z^+ \approx 8$ at $Re = 2.5 \cdot 10^4$ and $\Delta x^+ \approx 55$ and $\Delta y^+ \approx \Delta z^+ \approx 35$ at $Re = 1.58 \cdot 10^5$ and a wall-normal first spacing of $\Delta z^+ < 1$. The aforementioned grid resolution bases on a grid sensitivity study. For the qualification of the uncertainty of grid convergence, numerical uncertainty was determined by the GCI method [23] as recommended for CFD studies [24]. Here, DES simulations have been carried out for three grid sizes ($N_1 < N_2 < N_3$) of the TE rib-configuration at Reynolds number of $Re = 5.1 \cdot 10^4$, $Re = 1.1 \cdot 10^5$ and $Re = 1.58 \cdot 10^5$ with a refinement factor of $r_{21} = 1.19$ and $r_{32} = 1.3$ for $Re \leq 1.1 \cdot 10^5$ and $r_{21} = r_{32} = 1.3$ for $Re = 1.58 \cdot 10^5$, respectively, leading to grid resolutions of $N_3 = 2.8 \cdot 10^6$, $N_2 = 6.15 \cdot 10^6$ and $N_1 = 10.4 \cdot 10^6$ ($Re < 1.1 \cdot 10^5$) and $N_1 = 14.3 \cdot 10^6$ ($Re = 1.58 \cdot 10^5$). The Grid Convergence Index (*GCI*) and the extrapolated error (ϕ^{ext}) of the fine-grid solution in $\overline{Nu}_r$ and $\bar{f}$ are listed in Tab. 1. The fluid domain cell numbers of the grids for the TE, TR and TI rib-configuration, used in the present study, range from $N_1 = 10.4 \cdot 10^6$ to $10.5 \cdot 10^6$ hexahedral cells for $Re < 1.1 \cdot 10^5$ and from $N_1 = 14.3 \cdot 10^6$ to $14.9 \cdot 10^6$ for $Re = 1.58 \cdot 10^5$. The meshes are displayed in Figure 2.

Numerical Methods

Computations were performed by the commercial solver FLUENT V.15 [25]. Three-dimensional, compressible flow, energy and turbulence model equations are solved within the fluid domain and a simplified energy equation $\partial(E \cdot \rho)/\partial t = -\partial q_j/\partial x_j$ is solved within the solid region. Governing equations were solved by a segregated solver and the SIMPLE algorithm was applied for solving the pressure-velocity-field coupling. The convective terms of the momentum equation were the discretised by the bounded central differencing scheme. For the equations of turbulent kinetic energy, specific dissipation rate, density and energy second order upwind schemes were used. The diffusion terms were second order central difference and the pressure terms second order discretised. Temporal discretization were conducted by the bounded second order implicit scheme and gradients were Green-Gauss cell-based approximated.

Data Evaluation

The averaged Nusselt number at the rib-roughened wall $\overline{Nu}_r$ was calculated between the 13th and 14th rib-element from

$$\overline{Nu}_r = \frac{1}{\Delta t}\int_{\Delta t}\frac{1}{S_r}\int_{S_r} q_r/(T_r - \bar{T}_b) \cdot D_h/\kappa(\bar{T})\, dS_r\, dt \quad (1)$$

with the time-average interval Δt of fifty flow-throughs over one rib-section, the heat transfer area S_r between both rib-elements, the spatially averaged bulk fluid temperature $\bar{T}_b$ and fluid temperature $\bar{T}$. The overall Nusselt number $\overline{Nu}_c$ of the total channel surface S_c for one rib-section between the 13th and 14th rib-element was determined analogously. The friction factor was determined from the streamwise pressure drop Δp over the distance L and the averaged mass flow rate $\dot{m}$ between the 7th and 14th rib:

$$\bar{f} = \frac{1}{\Delta t} \int_{\Delta t} (\Delta p \cdot D_h \cdot \rho(\bar{T}) \cdot A^2)/(2 \cdot L \cdot \dot{m}^2)\, dt. \qquad (2)$$

It is noted that the flow was thermal-hydraulically fully developed within the analysed region of the present computational domain.

Experimental Setup for Validation Tests

The applied computational approach and method is validated against heat transfer and pressure drop measurement results of the experimental setup of HETREX. Experiments were carried out for comparable flow and heating conditions of the numerical simulations. For the sake of brevity, only the essentials of the experimental setup and measurement techniques are provided in the present publication. The experimental facility consists of the test section, a piping system and peripheral devices. The test section contains the channel and a heating unit and was made of stainless steel [X6CrNiMoTi17-12-2 (316Ti)]. The channel contains an unheated smooth inlet zone with a length of 500 mm, the heated test zone with a length of 300 mm and an unheated smooth outlet zone with a length of 50 mm. As mentioned above, the computational domain was derived from the experimental test section and, thus, the size of the test section and channel cross-section, the rib-elements and the structure material of the experimental and numerical setup are identical for e = 1 mm. The fluid flow was provided by a compressed air system and the mass flow rate and inlet pressure were regulated by a PID-controlled pneumatic valve integrated upstream the test section and manual valves located downstream the test section. The flow was conditioned by a static helical flow mixer, a honeycomb grid and a flow straightener installed upstream the test section. Constant heat flux density was supplied to the experiment by an electrical powered heater cartridge, Typ Graeff HLP custom-made, inserted into the heating unit. The fluid bulk temperatures were measured by PT100 thermocouples downstream of a flow conditioner at the test section inlet and downstream of a static helical flow mixer at the test section outlet. A linear bulk temperature distribution in axial direction was assumed for the rib-roughened zone. The mass flow rate was measured by an Endress & Hauser 80F Coriolis flow meter. The wall temperatures were measured at the heated channel wall by calibrated thermocouples and the static pressure distribution along the test section were measured by Honeywell FD2000 pressure sensors. The temperatures at the sheet metal cover and the ambient temperature were measured for determining the heat loss rate of the test section. Here, free convection was assumed to occur at the isolation layer and the heat loss rates of the cylindrical thermal isolation layer and the vertical end caps were calculated with determined heat transfer coefficients of free convection for horizontal cylinders and vertical plates.

RESULTS

Validation

For validation, the averaged friction factor ratio $\bar{f}/f_s$ - determined from the pressure drop measurements between the 7th and 16th rib - and the local Nusselt Number ratios $\overline{Nu_p}/Nu_s$ - based on pointwise measured temperatures between the 18th and 19th rib-element and a constant nominal heat flux density - including the experimental uncertainties are shown in Fig. 3, with the Dittus-Boelter Nusslet number correlation of $Nu_s = 0.023 \cdot Re^{0.8} \cdot Pr^{0.4}$ and the Blasius friction factor correlation of $f_s = 0.046 \cdot Re^{-0.2}$ for smooth circular channel flows. For comparison the corresponding computational Nusselt number ratio was determined between the 13th and 14th rib-element. The maximum experimental uncertainty of the present results [26] was estimated to be less than 4.8 pct. in the friction factor and to be less than 5.4 pct. in the Nusselt Number. The numerical results of the nominal Nusslelt Number ratios $\overline{Nu_p}/Nu_s$ agree well with the experimental data. The friction factor ratios derived by the numerical simulations differ slightly from the experiments, but are within the experimental uncertainty for most of the Reynolds number range.

Friction Factor and Nusslet Number

The averaged friction factor $\bar{f}$, the Nusselt Number $\overline{Nu_r}$ and $\overline{Nu_c}$ are displayed in Fig. 4 and 5. Based on the computational results, Reynolds number dependent power law correlations for the averaged friction factor and the Nusselt number were derived for $2.5 \cdot 10^4 \leq Re \leq 1.58 \cdot 10^5$,

$$\bar{f} = g_f \cdot Re^{-m} \pm 4\% \ (2.5 \cdot 10^4 \leq Re \leq 1.58 \cdot 10^5) \quad (3)$$

$$\overline{Nu_r} = g_{Nu_r} \cdot Re^{0.73} \pm 2\% \ (2.5 \cdot 10^4 \leq Re \leq 1.58 \cdot 10^5) \quad (4)$$

$$\overline{Nu_c} = g_{Nu_c} \cdot Re^{0.8} \pm 3\% \ (2.5 \cdot 10^4 \leq Re \leq 1.58 \cdot 10^5) \quad (5)$$

The coefficients are listed in Tab. 2 and the correlated distributions (interp.) and deviations are included in Fig. 4 and 5.

$\overline{Nu_r}$ and $\overline{Nu_c}$ increase and $\bar{f}$ decreases for increasing Reynolds numbers. Compared to previous investigations for turbulent flow in one-sided rib-roughened channels of p/e = 10 and e/D_h = 0.066 at Reynolds number of $Re \leq 5 \cdot 10^4$ [3], Nusselt numbers, $\overline{Nu_r} = 0.3678 \cdot Re^{0.571}$, are in a range of 5 pct. to 15 pct. Friction factor raise and heat transfer enhancement occur in the descending order of the rib-configurations: TE, TR and TI. The flow moves smoother over the rib-elements with inclined and round-edged rib-surface than over the 90° edged one. The rate of change of flow acceleration and deceleration decrease and the pressure and velocity gradients are reduced and smoothed. The friction and heat transfer enhancement reduction are assumed to be caused by (A) decreased vertical and lateral flow motion close to the rib-element, (B) decreased flow separation at the leading- and rear-edge of rib-top-surface, (C) reduced impingement of turbulent flow structures on the channel wall at the shear layer reattachment region and on the successive rib further downstream, (D) lower turbulence levels and (E) reduced secondary flow motion. It is assumed that the differences and similarities can be attributed to the aforementioned thermal- hydraulic effects (A)-(E) that contribute with various extents to flow resistance and heat transfer development for different rib- shapes. Whereas heat transfer enhancement is related to flow effects causing turbulence kinetic energy raise [4], the friction factor is primarily dominated by the form drag of the rib-elements [1,6]. As displayed in Fig. 6 the turbulence kinetic energy $k = 0.5 \cdot \left(\overline{u_i'^2}\right)$ is decreased for the TR and TI rib-configuration and in a comparable range, with the velocity fluctuation u_i' in direction *i*. Thus, in contrast to the friction factor, both Nusselt numbers, $\overline{Nu}_r$ and $\overline{Nu}_c$, are similar for the TR and TI rib-configuration and distinctly offset to the TE rib- configuration.

Friction Factor and Nusselt Number Ratio

The computed and correlated distributions of the friction factor ratios, $\bar{f}/f_s$, the Nusselt Number ratios at the rib-roughened wall, $\overline{Nu}_r/Nu_s$, and the overall Nusselt number ratios of the channel, $\overline{Nu}_c/Nu_s$, for varying Reynolds numbers are displayed in Fig. 3. Analogous to previous studies [1,11-13], the heat transfer enhancement correlates with the raise of rib-induced flow resistance and heat transfer ratio at the rib-roughened wall, $\overline{Nu}_r/Nu_s$, decreases and friction factor ratio, $\bar{f}/f_s$, increases for increasing Reynolds numbers. $\overline{Nu}_c/Nu_s$ remains nearly constant for the entire Reynolds number range. The friction factor ratios are significantly effected by the rib-shapes, whereas the heat transfer ratios differ marginally. Similar effects have been reported for rib-elements of semi- circular, triangular an trapezoid rib-shapes [14,16]. Maximum rib-induced flow resistance occurs for the TE rib-configuration and the friction factor is raised about 2.9-3.3 times, compared to the Blasius smooth channel flow. A slightly reduced friction factor development is obtained for the TR rib-configuration with ratios of 2.9-3.1. Minimum friction factors are generated by TI rib-configuration with $\bar{f}/f_s$ of about 2.5 for the entire Reynolds number range. The friction factor ratios for the TE or TR and the TI rib-configuration drift apart for increasing Reynolds numbers. The Reynolds number dependency of $\overline{Nu_r}/Nu_s$ is in a comparable range for the three channel designs and the ratios decrease for increasing Reynolds numbers. Maximum heat transfer occurs for the TE rib-configuration. Compared to thermal-hydraulics of smooth circular channels, the corresponding heat transfer at the rib-roughened wall is enhanced about 1.9 times at $Re = 2.5 \cdot 10^4$ and about 1.7 times at $Re = 1.58 \cdot 10^5$. The Nusselt numbers ratios for TR and TI differ slightly and ranges from $\overline{Nu_r}/Nu_s = 1.7$ at $Re = 2.5 \cdot 10^4$ to $\overline{Nu_r}/Nu_s = 1.5$ at $Re = 1.58 \cdot 10^5$. The overall Nusselt number ratios $\overline{Nu_c}/Nu_s$ are in the range of 1.15 to 1.25 for all rib-configurations.

Thermal Performance

The price paid for heat transfer enhancement is the large increase in flow resistance and the thermal performance of rib-roughened internal cooling passages have to be evaluated by the design criteria of increased heat conductance K/K_s, reduced pumping power P/P_s and reduced heat transfer area S/S_s [27], compared to smooth circular channel flows. Moreover, it is proposed to differentiate the evaluation criteria between the performance factor for cooling the rib-roughened wall and the overall performance factor based on a rib-section. Increased heat conductance (for equal pumping power and heat transfer area) K_r/K_s and K_c/K_s vs. Re are displayed in Fig. 7. The overall performance factor varies in the range of $0.84 < K_c/K_s < 0.88$, $0.83 < K_c/K_s < 0.84$ and $0.85 < K_c/K_s < 0.87$ for the TE, TR and TI rib-configuration. The benefit of the overall heat transfer enhancement is reversed by the accompanied pumping power raise. However, improved thermal performances for cooling the rib-roughened wall were obtained for all rib-shapes. Similar to previous studies [13], K_r/K_s decreases for increasing Reynolds numbers. The Reynolds number dependency is similar for the TE and TR rib-configuration and is reduced for the TI rib-configuration. K_r/K_s ranges from 1.14 to 1.34, from 1.11 to 1.24 and from 1.03 to 1.23 for the TE, TR and TI rib- configuration. Best performance factors for cooling the rib-roughened wall was obtained for the TE rib-configuration.

CONCLUSION

The thermal-hydraulics of a one-sided heated, rib-roughened cooling channel (p/e = 10, e/D_h = 0.0638) with three different rib-shapes at $2.5\cdot 10^4 \leq Re \leq 1.58\cdot 10^5$ were analysed. The following conclusions can be drawn:

(1) The applicability of the computational methods for predicting the averaged friction factor and Nusselt numbers were validated against experimental data. The numerical results of the Nusselt numbers agree well with the experimental data and the averaged friction factors are within the experimental uncertainty for the entire Reynolds number range.

(2) Maximum flow resistance and heat transfer occurs for the TE rib-configuration (90 deg. edged, square rib-element). Compared to the smooth channel flow, the friction factor is raised about 2.9-3.3 times and the Nusslet number is increased about 1.7-1.9 times.

(3) Reynolds number dependent power law correlations for the averaged friction factor $\bar{f}$ and the Nusselt number $\overline{Nu}_r$ and $\overline{Nu}_c$ were derived.

(4) The averaged friction factor ratio differs up to 28 pct. for varying rib-shapes, whereas the averaged Nusslet Number ratios at the rib-roughened wall differ up to 12 pct.

(5) Differences and similarities of Nusselt numbers and averaged friction factor for varying rib-shapes are assumed to be attributed to thermal-hydraulic effects that contribute with various extents to flow resistance and heat transfer development.

(6) Improved thermal performance for cooling the rib-roughened wall occurred for all rib-shapes.

(7) Best thermal performances was obtained for the TE rib-configuration, $1.14 < K_r/K_s < 1.34$.

NOMENCLATURE

A	[m^2]	Channel cross section
c_p	[J/kg·K]	Specific heat capacity
C_{DES}^k	[-]	DES Constant
D_h	[m]	Hydraulic diameter
e	[m]	Rib-height
E	[J/kg]	Total energy per unit mass
$\bar{f}$	[-]	Averaged friction factor
f_s	[-]	Smooth channel friction factor
g_f, g_{Nu}	[-]	Coefficients
k	[m^2/s^2]	Turbulence kinetic energy

K/K_s	[-]	Increased heat conductance ratio
l	[m]	Length scale
L_e	[m]	Rib-length
$\dot{m}$	[kg/s]	Mass flow rate
$\overline{Nu}$	[-]	Averaged Nusselt Number
Nu_s	[-]	Smooth channel Nusselt Number
p	[m]	Pitch
P/P_s	[-]	Reduced pumping power ratio
p_{in}	[Pa]	Inlet Pressure
Pr	[-]	Prandtl Number
Δp	[Pa]	Pressure Drop
q^+	[-]	Dimensionless heat up rate
q	[W/m^2]	Heat flux
Re	[-]	Reynolds number
S	[m^2]	Heat transfer area
S/S_s	[-]	Reduced heat transfer area ratio
T	[K]	Temperature

T_{in}	[K]	Inlet temperature
T_b	[K]	Bulk Temperature
Δt	[s]	Integration time interval
u	[m/s]	Streamwise flow velocity
x	[m]	Coordinate
$\Delta x, y, z$	[m]	Local grid size
$\Delta x^+, y^+, z^+$	[-]	Non-dimensional coordinates in x,y,z -direction

Greek symbols

κ	[W/m·K]	Thermal conductivity
ρ	[kg/m^3]	Density
ν	[m^2/s]	Viscosity
ε	[m^2/s^3]	Turbulent dissipation rate
ω	[1/s]	Spec. turbulent dissipation rate
β^*	[-]	Model constant
Δ	[m]	Filter width

Subscripts

c	Channel wall of one rib-section
j	*j*=1,2,3 cartesian axis direction
m	Mean
r	Rib-roughened wall
s	Smooth circular channel
SGS	Subgrid Scale
t	Turbulent

REFERENCES

[1] Rau G., Cakan M., Moeller D., and Arts T., The Effect of Periodic Ribs on the Local Aerodynamic and Heat Transfer Performance of a Straight Cooling Channel, *Journal of Turbomachinery*, vol. 120, pp. 368-375, 1998.

[2] Liou T.-M., Hwang J.-J., and Chen S.-H., Turbulent Transport Phenomena in a Channel with Periodic Rib Turbulators, *Journal of Thermophysics and Heat Transfer*, vol. 6, no. 3, pp. 513-521, 1992.

[3] Liou T.-M., Hwang J.-J., Chen S.-H., Simulation and measurement of enhanced turbulent heat transfer in a channel with periodic ribs on one principal wall*, International Journal of Heat and Mass Transfer*, vol. 36, no. 2, pp. 507-517, 1993.

[4] Liou T.-M., and Hwang J.-J., Turbulent Heat Transfer Augmentation and Friction in Periodic Fully Developed Channel Flows, *Journal of Heat Transfer*, vol. 114, no. 1, pp. 56-64, 1992.

[5] Labbé O., Large-eddy-simulation of flow and heat transfer in a ribbed duct, *Computers & Fluids*, vol. 76, pp. 23-32, 2013.

[6] Tafti D.K., Evaluating the role of subgrid stress modeling in a ribbed duct for the internal cooling of turbine blades, *International Journal of Heat and Fluid Flow*, vol. 26, pp. 92-104, 2005.

[7] Sewall, E.A., Tafti D.K., Graham, A.B., Thole K.A., Experimental validation of large eddy simulations of flow and heat transfer in a stationary ribbed duct, *International Journal of Heat and Fluid Flow*, vol. 27, pp. 243-258, 2006.

[8] Viswanathan A.K, and Tafti D.K., Detached Eddy Simualtion of Turbulent Flow and Heat Transfer in a Ribbed Duct, *Journal of Fluids Engineering*, vol. 127, pp. 888-896, 2005.

[9] Viswanathan A.K, Tafti D.K., Detached eddy simulation of turbulent flow and heat transfer in a two-pass internal cooling duct, *International Journal of Heat and Fluid Flow*, vol. 27, pp. 1-20, 2006.

[10] Han, J.C., Heat Transfer and Friction in Channels With Two Opposite Rib-Roughened Walls, *Journal of Heat Transfer*, vol. 106, pp. 774-781, 1984.

[11] Han, J.C., Heat Transfer and Friction Characteristics in Rectangular Channels With Rib Turbulators, *Journal of Heat Transfer*, vol. 110, pp. 321-328, 1988.

[12] Han, J.C., Zhang Y.M., and Lee C.P., Augmented Heat Transfer in Square Channels With Parallel Crossed, and V-Shaped Angled Ribs, *Journal of Heat Transfer*, vol. 113, pp. 590-596, 1991.

[13] Chandra P.R., Alexander C.R., and Han, J.C., Heat transfer and friction behaviors in rectangular channels with varying number of ribbed walls, *International Journal of Heat and Mass Transfer*, vol. 46, pp. 481-495, 2003.

[14] Han, J.C., Glicksman L., and Rohsenow W.M., An Investigation of Heat Transfer and Friction for Rib-Roughened Surfaces, *International Journal of Heat and Mass Transfer*, vol. 21, pp. 1143-1156, 1978.

[15] Han J.C., and Park J.S., Developing heat transfer in rectangular channels with rib turbulators, *International Journal of Heat and Mass Transfer*, vol. 31, no. 1, pp. 183-195, 1988.

[16] Liou T.-M., and Hwang J.-J., Effect of ridge shapes on turbulent heat transfer and friction in a rectangular channel, *International Journal of Heat and Mass Transfer*, vol. 36, no. 4, pp. 931-940, 1996.

[17] Spalart P.R., Jou W.H., Strelets M., and Allmaras S.R, Comments on the Feasibility of LES for Wings and on a Hybrid RANS/LES Appraoch, Advances in DNS/LES, *Proceedings of the 1st AFOSR International Conference on DNS/LES*, pp. 137-147, 1997.

[18] Strelets, M.Kh., Detached Eddy Simulation of Massively Separated Flows, *AIAA Paper*, 2001-0879, pp. 1-18, 2001.

[19] Travin A., Shur M., Strelets M.Kh., and Spalart P. R., Physical and Numerical Upgrades in the Detached-Eddy Simulation of Complex Turbulent Flows, *Advances in LES of Complex Flows*, vol. 65, pp. 239-254, 2002.

[20] Menter F. R., Two-Equation Eddy-Viscosity Turbulence Models for Engineering Applications, *AIAA Journal*, vol. 32. No. 8, pp. 1598-1605, 1994.

[21] Spalart P.R., Deck S., Shur M.L., Squires K.D., Strelets M.Kh., Travin A., A new version of detached-eddy simulation, resistant to ambiguous grid densities, *Theoretical and Computational Fluid Dynamics*, vol. 20, pp. 181-195, 2006.

[22] VDI, Heat Atlas, Springer-Verlag Berlin Heidelberg, 2, 2010.

[23] Roache, P. J., Perspective: A Method for Uniform Reporting of Grid Refinement Studies, *Journal of Fluids Engineering*, vol. 116, no. 3, pp. 405-413, 1994.

[24] Procedure for Estimation and Reporting of Uncertainty Due to Discretization in CFD Applications, *Journal of Fluids Engineering*, vol. 130, no. 7, 2008.

[25] ANSYS Fluent Theory Guide, Release 15.0, 2013.

[26] Kline S. J., and McClintock F. A., Describing uncertainties on single-sample experiments, *Mechanical Engineering*, vol. 9, no. 57, pp. 3-8, 1953.

[27] Gee D.L., Webb R.L., Forced Convection Heat Transfer in Helically Rib-Roughened Tubes, *International Journal of Heat and Mass Transfer*, vol. 23, pp.1127-1136, 1980.

Table 1: Grid Convergence Index and extrapolated error

Uncertainty [pct.]			
Re	$5.1 \cdot 10^4$	$1.1 \cdot 10^5$	$1.58 \cdot 10^5$
$GCI_{Nu_r}^{21}$	1.61	2.98	1.62
$\phi_{Nu_r}^{ext}$	1.29	2.38	1.30
$GCI_{\bar{f}}^{21}$	0.44	1.02	0.58
$\phi_{\bar{f}}^{ext}$	0.35	0.81	0.47

Table 2: Coefficients of the Correlations

Coefficients	Rib-configurations		
	TE	TR	TI
g_f	0.072	0.077	0.103
m	0.14	0.15	0.19
g_{Nu_r}	0.077	0.071	0.07
g_{Nu_c}	0.025	0.024	0.024

List of Figure Captions

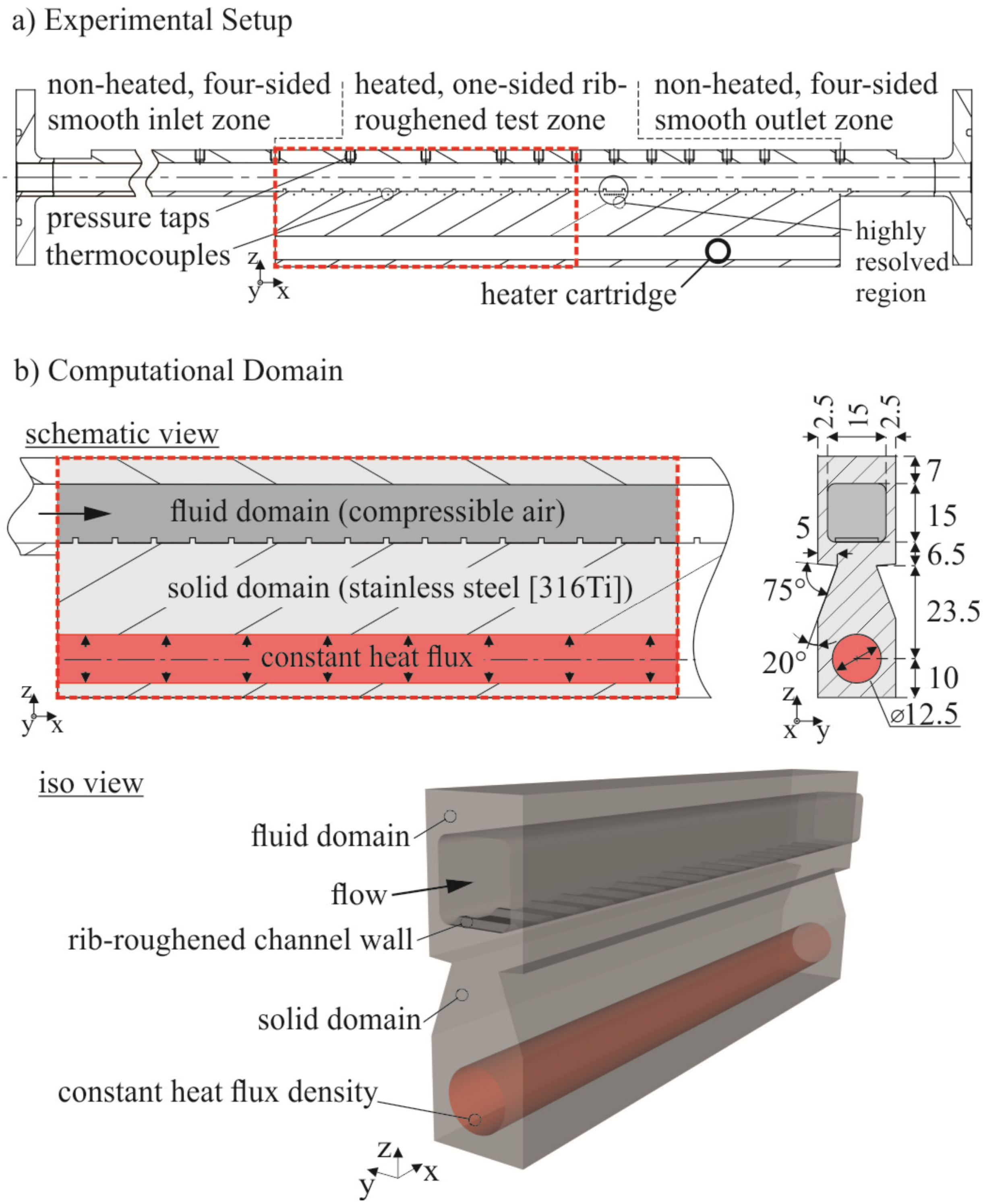

Figure 1 HETREX (a) experimental setup and (b) computational domain.

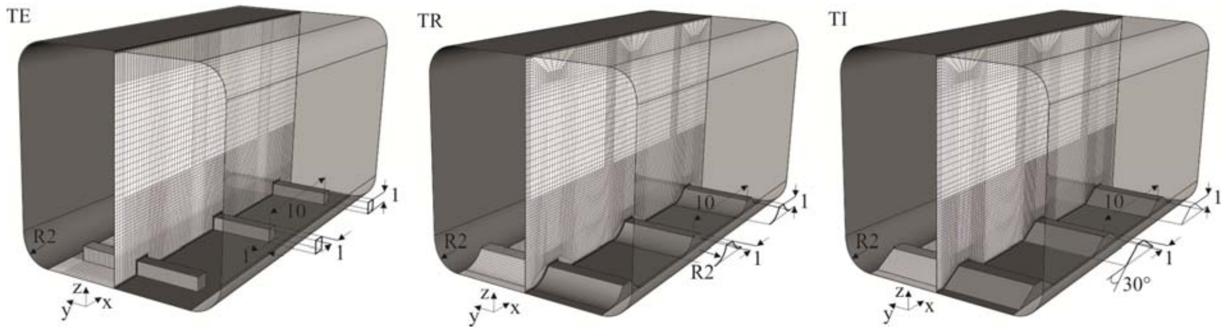

Figure 2 TE, TR and TI rib-configuration

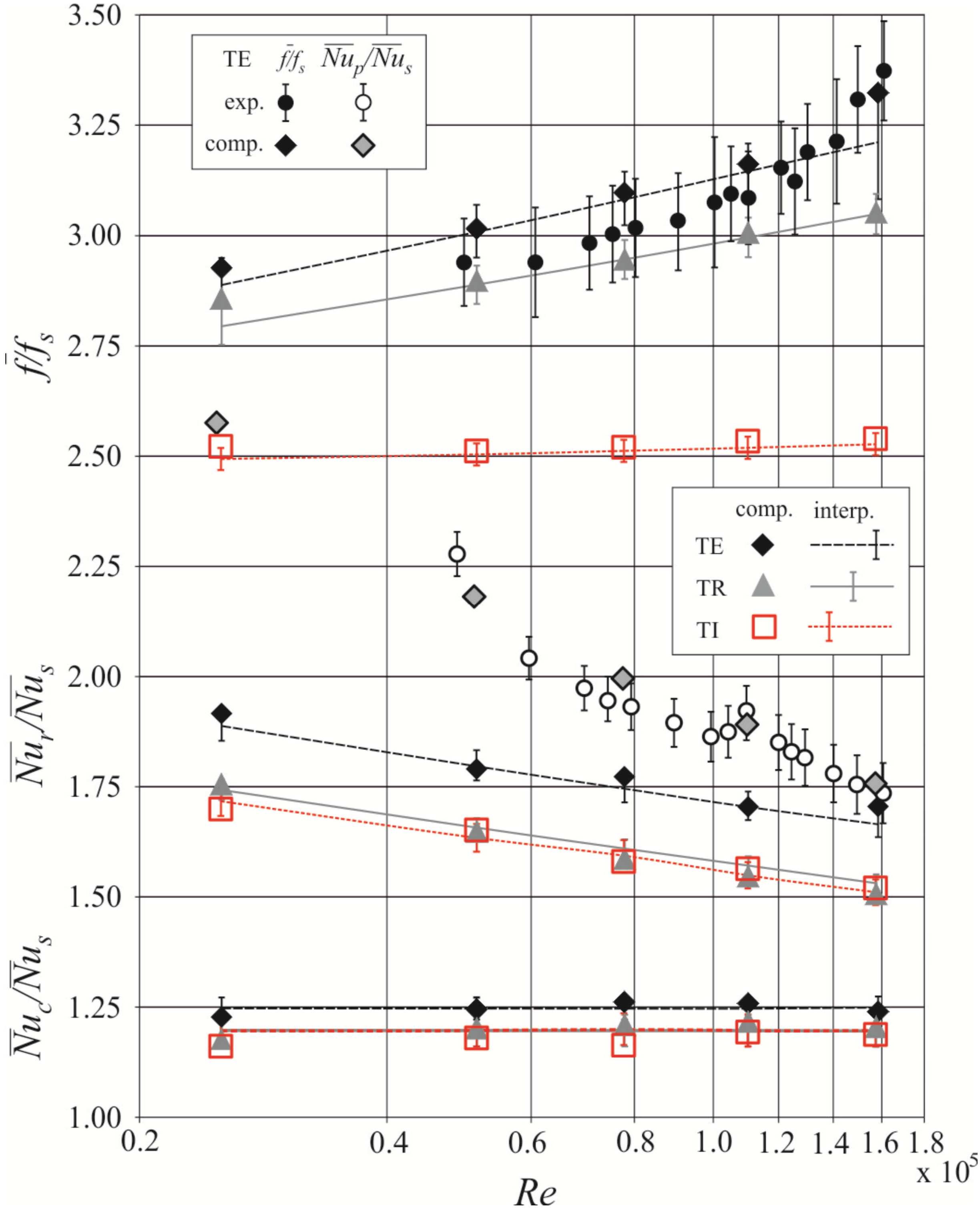

Figure 3 Averaged friction factor ratios and Nusselt Number ratios.

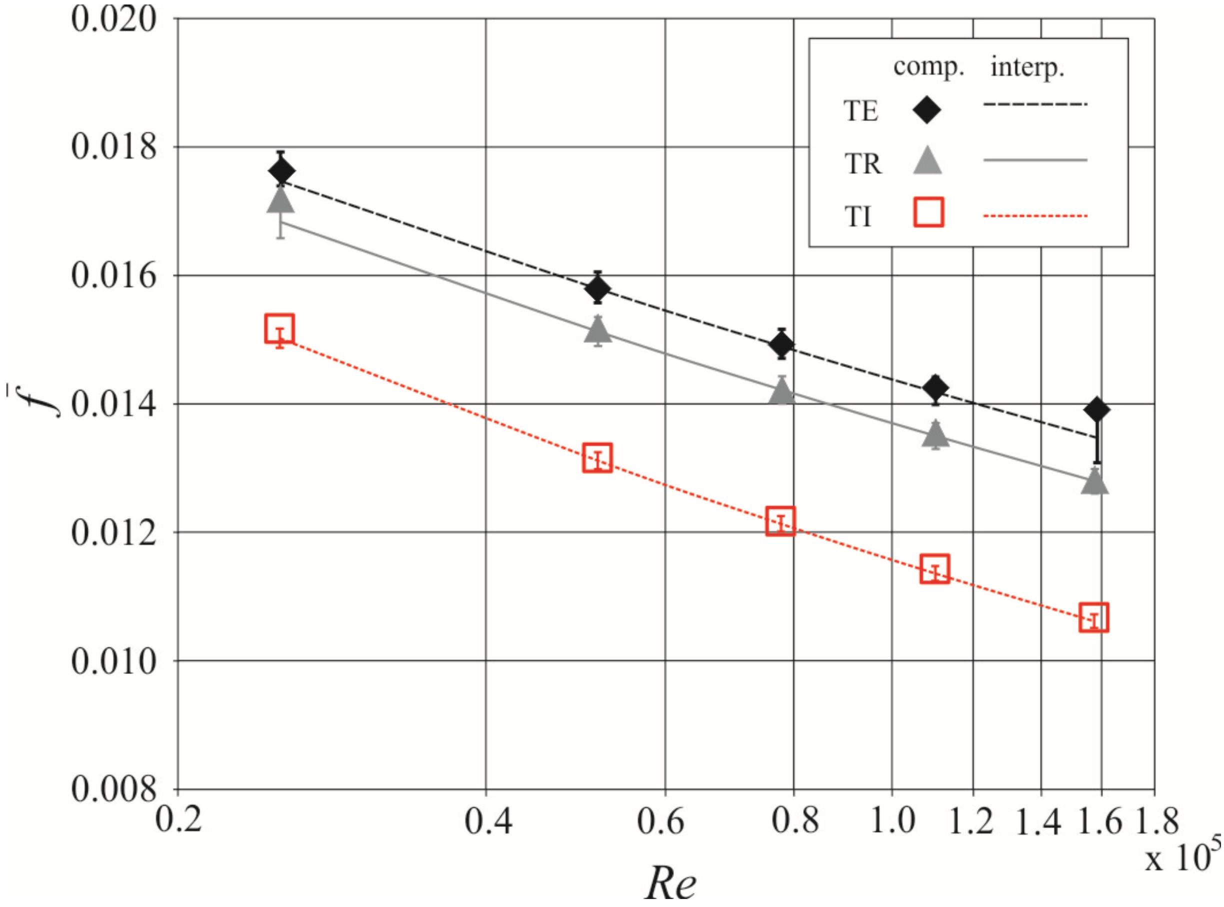

Figure 4 Averaged friction factor vs. Reynolds numbers.

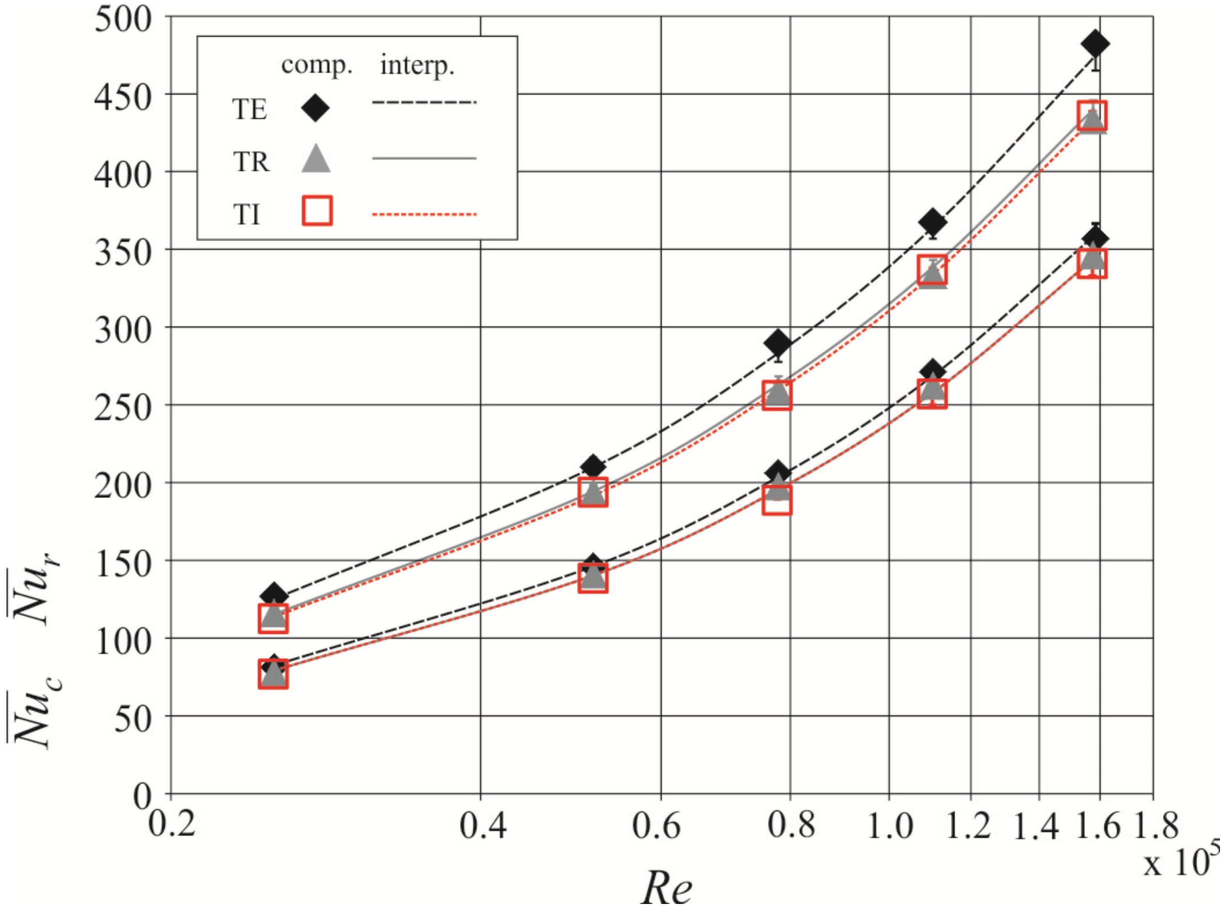

Figure 5 Nusselt Numbers at the rib-roughened wall and of the channel vs. Reynolds numbers.

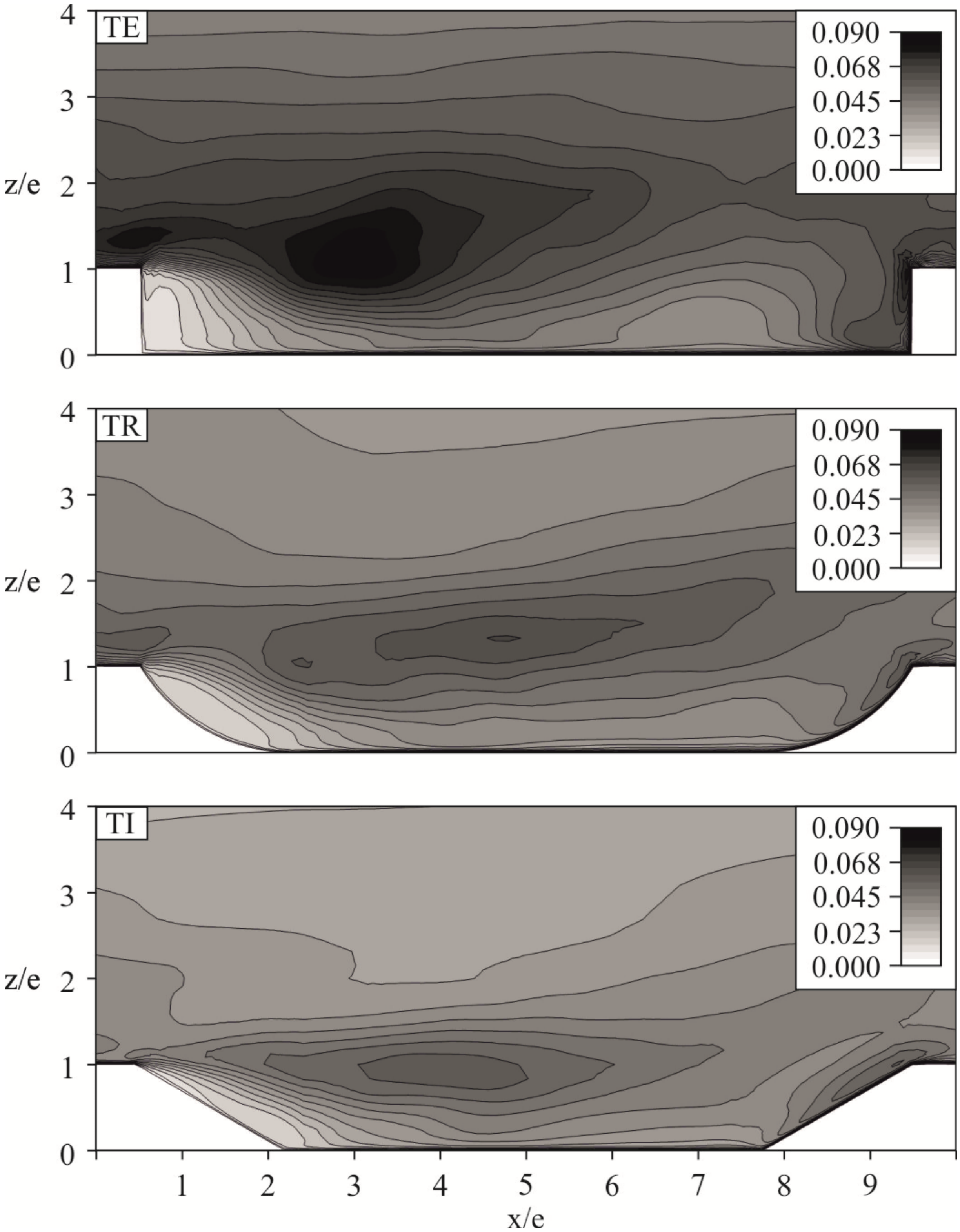

Figure 6 Normalized turbulence kinetic energy k/u_m^2 at the center plane of the channel for the TE, TR and TI rib-configuration.

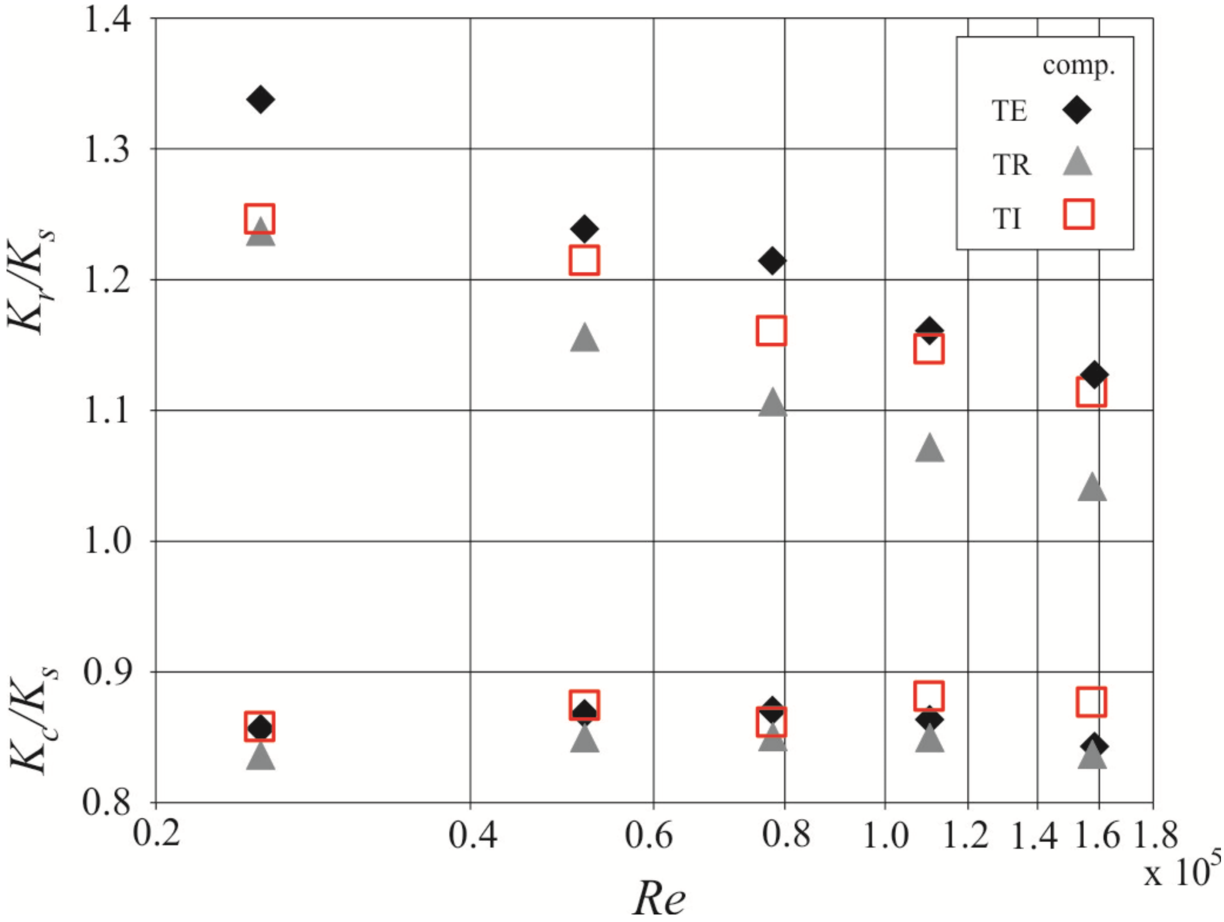

Figure 7 Increased heat conductance (for equal pumping power and heat transfer area) vs. Reynolds numbers.